ChemPubSoc Europe

DOI: 10.1002/celc.201500122

CHEMELECTROCHEM Articles

Special Issue

High-Temperature, In Situ X-ray Absorption Study of Sr_2MgMoO_6 Solid-Oxide Fuel-Cell Anode Materials

Bryan C. Eigenbrodt,*[a] Anthony M. Young,[b] Thomas G. Howell,[b] Carlo U. Segre,[c] and Thomas L. Reitz[b]

Limitations of current solid oxide fuel cell anode materials have spurred the exploration of alternative materials. Mixed ionic and electronic conducting anode materials have the potential to overcome these limitations. The mixed ionic and electronic conducting material explored in this work is Sr_2MgMoO_6 (SMMO). X-ray absorption spectroscopy in conjunction with an in situ assembly was used to study the fundamental redox chemistry of SMMO at 800 °C. The X-ray absorption spectra for the Mo K-edge exhibited changes in the reduced and oxidized bulk SMMO samples, as evident in a shift in the Mo binding energies and in the formation of oxide vacancies. However, in situ measurements of the working devices revealed that the Mo oxidation state remained unchanged under various cell polarizations. These findings demonstrate that SMMO, as a solid oxide fuel cell anode, has the potential to provide adequate electron conduction through multivalent Mo sites and to provide fuel tolerance through oxide vacancies built into its crystal structure.

1. Introduction

With the current deteriorating state of our environment coupled with an increasing demand on the limited supply of fossil fuels, finding technologies that utilize renewable resources efficiently while generating minimal pollution is a priority of any national energy policy. One of these technologies is the fuel cell, specifically the solid oxide fuel cell (SOFC), which has attracted considerable attention because of its ability to provide electricity cleanly and efficiently.[1–4] These electrochemical devices can convert a wide variety of fuels (e.g. H_2, CO, alkanes, and alcohols) into products and electricity with efficiencies as high as 80% in combined heating and power applications.[1–3] If these devices operate on hydrocarbon-based fuels, they will generate pollutants (e.g. CO, CO_2, nitrogen oxides, and sulfur oxides), but because they operate at such high fuel efficiencies, the environmental impact is minimal.[1–3]

SOFCs consist of a solid oxide electrolyte and two electrodes: an anode and a cathode. Currently used anodes typically consist of a porous electrocatalyst composite consisting of nickel intermixed with the electrolyte material, also known as ceramic–metallic (cermet) composites.[1–3] The cathode of an SOFC typically consists of an electrocatalytic material such as lanthanum strontium manganate.[1,5,6] In the most general sense, the overall chemistry occurring in SOFCs results in electrochemical oxidation of the fuel, which gives rise to the production of oxide products (i.e. H_2O and CO_2) and electricity via oxide anions that have already been electrochemically reduced at the cathode.[1,3,7,8] The oxide anions arrive at the anode after diffusing through oxide vacancies in the electrolyte crystal matrix.[9–13] Oxidation of the fuel is thought to happen at the three-phase boundary (TPB), the region in which the ionically conducting electrolyte, the electronically conducting anode, and the gas-phase fuel mixture all meet.[14–20] At the TPB, electrons are carried away into the circuit and arrive at the cathode where they reduce the adsorbed oxygen atoms to form oxygen anions to complete the circuit.[2,9,7,14]

The high activation energies required to drive oxide diffusion through the electrolyte (100 kJ mol^{-1}) and to activate molecular oxygen at the cathode (223 kJ mol^{-1}) require that SOFCs operate at relatively high temperatures ($\geq$650 °C) to generate appreciable currents.[21,22] In these environments, the complex chemistry of hydrocarbon fuels leads to degradation of the anode catalyst, which results in the eventual failure of the SOFC device.[7] At high temperatures, higher molecular weight hydrocarbon fuels undergo gas-phase pyrolysis to form unsaturated precursors that nucleate graphite growth in the Ni anode microstructure and block catalytically active Ni sites.[3,23] In addition, the high sulfur content in many hydrocarbon fuels, such as natural gas, permits the reaction of H_2S with Ni to form NiS.[24–26] Just like with graphite, once sulfidation of the nickel lattice occurs, the lower melting points of these sulfides (NiS m.p. = 797 °C) result in detrimental rearrangement of the anode microstructure.[24–26] This breakdown of the anode mi-

[a] Prof. B. C. Eigenbrodt
Department of Chemistry
Villanova University
800 E. Lancaster Avenue, Villanova, PA 19085 (USA)
E-mail: bryan.eigenbrodt@villanova.edu

[b] A. M. Young, Dr. T. G. Howell, Dr. T. L. Reitz
Aerospace Systems Directorate
Air Force Research Laboratory
Wright Patterson Air Force Base, OH 45433 (USA)

[c] Prof. C. U. Segre
Physics Department and CSRRI
Illinois Institute of Technology
Chicago, IL 60616 (USA)

Special Issue An invited contribution to a Special Issue on In Situ Monitoring of Fuel Cell and Battery Processes

crostructure will negatively impact anode porosity, fuel tortuosity, and the overall connectivity of the conducting anode network, all of which will lead to device degradation and eventual failure with prolong exposure to the fuel.[27] These limitations of SOFC technology have spurred the investigation of new mixed ionic and electronic conducting (MIEC) anode materials that are effective at blocking carbon deposits and sulfur formation while still maintaining electrocatalytic activity and electronic conductivity.[24–26]

In these oxygen-rich MIEC materials, high oxide anion mobility increases the resistance to carbon deposition and metal sulfide formation by promoting the oxidation reactions of incident fuel fragments to form CO, CO_2, SO, and SO_2.[24–26] Of the MIEC materials that have been investigated as promising candidates for SOFC anodes, those having a perovskite structure have shown the greatest potential for having long-term stability under standard SOFC operating conditions.[24–26] Perovskites adopt a ABO_3 composition, for which "A" represents a rare earth metal and "B" represents a transition or alkali earth metal.[24–26] These MIEC materials show sufficient ionic conductivity and minimal thermal expansion, which make them compatible with a wide variety of electrolyte materials.[24,25] However, the catalytic activity and electronic conductivity of perovskites are inferior to those of standard Ni-based cermet anodes.[24–26] Conversely, perovskites have the ability to accommodate oxide anion vacancies and limited stoichiometric variation in the crystal structure while still maintaining their structural stability.[24–26] These abilities allow perovskites to be tuned for catalytic activity by inducing either n-type or p-type conductivity with the addition of various dopants into the A sites and B sites of the crystal system, $A'_{1-a}A''_aB'_{1-2\delta}B''_{2\delta}O_{3-a/2+\delta}$.[24–26] Perovskites can also take on the configuration of $A_2B'_{1-x}B''_xO_{6-\delta}$ to become double perovskites. The double perovskite configuration allows the incorporation of 4d and 5d block elements to provide a mixed-valent system, in the "B" site, which can result in an enhancement in electron conduction. The material under investigation in this paper will be the double perovskite Sr_2MgMoO_6 (SMMO). The molybdenum in SMMO has the unique capability to adopt multiple oxidation states (Mo^{VI}, Mo^{V}, and Mo^{IV}) while still maintaining its coordination chemistry.[24–26] Therefore, the focus of the research presented will be to explore the changes in the Mo oxidation state in SMMO as a function of the operation conditions of the SOFC.

Investigating and understanding the chemical reactions and processes that occur at the electrodes in these devices can prove to be a daunting task. Most of the challenges associated with SOFC research are related to the operational conditions and the design of the devices themselves.[2,14,28] The high operating temperatures (>650 °C) and inaccessible architectures make it extremely challenging to validate proposed kinetic models because of lingering questions regarding elementary reactions occurring in the SOFC during operation. Current methods used to study these devices involve the use of standard electrochemical measurements.[29–32] These methods can provide valuable information about changes in performance, as the operating conditions of the device change. Other research efforts involve the use of ex situ characterization measurements in conjunction with electrochemical measurements to provide indirect information about chemical species or material changes that occur during operation. Given that ex situ measurements are conducted after the device has been brought to room temperature and disassembled, they cannot provide a direct correlation between changes in electrochemical performance with specific chemical and material changes that occur in the SOFC during operation. Having the ability to conduct in situ measurements can provide unparalleled insight into SOFC chemistry that could not normally be obtained from standard ex situ measurements.

The experiments presented involved the use of in situ fluorescence-based X-ray absorption spectroscopy (XAS) measurements in combination with electrochemical characterization to overcome the challenges associated with performing in situ studies of SOFC chemistry. The ability to conduct XAS measurements will provide an opportunity to explore the role and behavior of these alternative MIEC anode materials in real time and under standard SOFC operational conditions. Specifically, these in situ XAS measurements will investigate changes in the oxidation state of Mo and changes in the concentration of oxygen atoms in these MIEC materials under varying operation conditions. This objective was accomplished by using a unique, custom built electrochemical assembly that was coupled with the X-ray absorption spectrometer at the Material Research Collaborative Access Team (MR-CAT)-10-ID beamline at Argonne National Laboratory's Advanced Photon Source (APS).

2. Results and Discussion

2.1. Redox Chemistry of SMMO

Prior to exploring the effects that electrochemical polarization and oxide flux will have on the SMMO electrode in working SOFC devices, the bulk redox chemistry of SMMO was first investigated to provide a diagnostic for the in situ measurements. This was accomplished by using a custom in situ XAS chamber to heat up an SMMO pellet to 800 °C and then exposing the sample to either oxidizing or reducing environments. At first, the SMMO pellet was heated to 800 °C under a 3% H_2 atmosphere and was dwelled there for 1 h to ensure that a completely reduced state was reached. After the dwell period, X-ray energy in the range of 19.8 to 20.1 keV was used to observe the Mo K-edge of our SMMO material. The resulting XAS data for the reduced SMMO sample can be seen in Figure 1.

There are three main components to the X-ray absorption spectrum, as highlighted in Figure 1a. These three components will be used to investigate the electronic and structural features of SMMO and will be the focus of this work. The "pre-edge" and "edge" fragments of the spectrum together represent the X-ray absorption near-edge structure (XANES) component of the data. XANES can provide information about the electronic structure of a material that is specifically associated with formal oxidation states and coordination chemistry.[33,34] In this work, the Mo K-edge was observed, and this correlates to

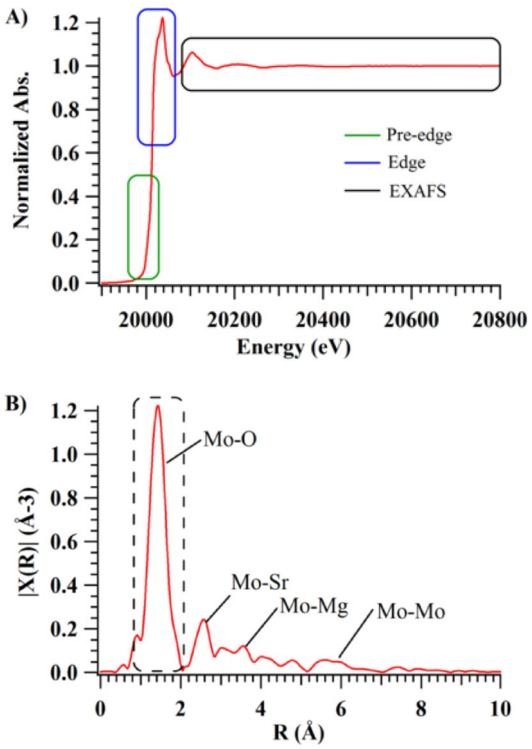

Figure 1. a) XAS Mo K-edge spectrum of reduced SMMO taken at 800 °C. The three specific areas of the spectrum are highlighted: pre-edge region (green), XANES region (blue), and EXAFS region (black). b) *R*-space spectrum generated from the Fourier transform of the EXAFS data with peak assignments of surrounding atoms with the excited Mo atom. The interaction of the Mo atom with surrounding O atoms is highlighted.

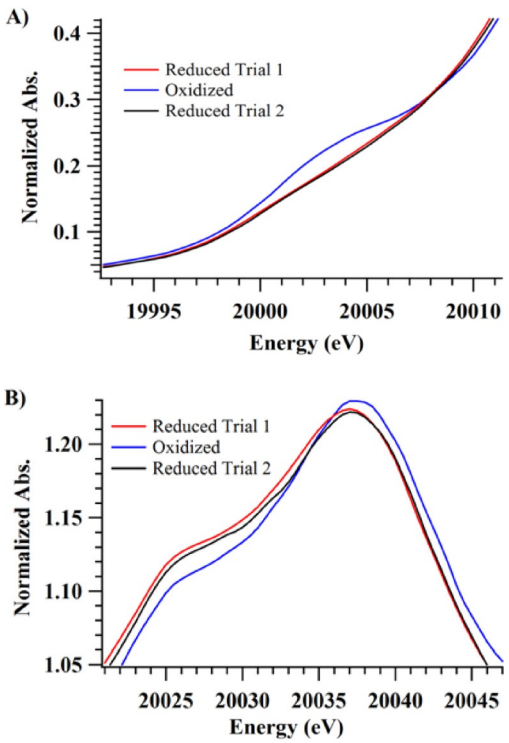

Figure 2. XANES spectra of the reduced (trial 1), oxidized, and reduced (trial 2) SMMO sample. a) Spectra of the "pre-edge" region and b) spectra of the "edge" region.

the energy needed to excite an electron to undergo a 1s→4p transition. This information will show up in the "edge" portion of the spectrum. There can also be restricted transitions that show up in the "pre-edge" region of the spectrum that are associated with a 1s→3d transition. The last segment of the X-ray absorption spectrum is associated with the scattered photoelectrons leaving the Mo atom and interfering, constructively and destructively, with neighboring atoms within the crystallographic matrix. This portion of the spectrum is referred to as the extended X-ray absorption fine structure (EXAFS). The pertinent information gained from the EXAFS data can be related to effective bond distances (R_{eff}), coordination number, and the types and nature of the neighboring atoms. By conducting a Fourier transform of the EXAFS data, the "*R*-space" spectrum is obtained (Figure 1b), and it provides information about the probability of neighboring atoms to the molybdenum atom as a function of R_{eff}. As a result of conducting these measurements at elevated temperatures, the peaks after $R=$ 4 Å show a significant decrease in the signal-to-noise ratio brought upon by the Debye–Waller factor.[35] The most intense peak that occurs at $R=1.5$ Å is associated with Mo–O interactions and will be the emphasis of this paper in trying to understand the extent of oxide vacancy formation about the Mo atom.

While still at 800 °C, the XAS chamber was evacuated with helium to remove any hydrogen before exposing the sample to air to collect data for the oxidized SMMO sample. Continuous spectra were taken to monitor the end of this oxidation process. To test the reversibility of the material, the chamber was evacuated of air and then once again exposed to the same reducing environment. The resulting data from this experiment can be seen in Figure 2. It is observed from these spectra that the change in the Mo oxidation state is a completely reversible process.

Upon monitoring the "pre-edge" of the XANES component of the spectrum (Figure 2a), it was observed that a feature started to emerge with prolong exposure to an oxidizing environment. As described above, this peak is associated with the restricted 1s→3d electron transition. This pre-edge feature arises from mixing of the oxygen 2p orbital with the molybdenum 3d orbital, which lowers its energy and allows the non-allowed $\Delta l \pm 2$ transition.[36] Upon oxidizing the SMMO sample, the oxygen concentration around the Mo atom increases due to oxide vacancies becoming filled. Filling in these oxide vacancies would only increase the mixing of these two orbitals to permit the non-allowed transition. Also in Figure 2a, it is observed that if the SMMO sample is exposed to the reducing environment once again, this pre-edge feature disappears to the original position of the first reduced trial and exhibits signs of a decrease in the mixing of the oxygen 2p and molybdenum 3d orbitals, signifying a decrease in the oxygen probability around the Mo atom, which is also a reversible process.

By investigating the "edge" section of the XANES component of the X-ray absorption spectrum (Figure 2b), observable changes can be seen for the Mo oxidation state upon switch-

ing from reducing to oxidizing environments. There are two features to this edge that are associated with the peaks of the low-spin and high-spin electron transitions the $1s \rightarrow 4p_{1/2}$ ($\approx$20025 eV) and $1s \rightarrow 4p_{3/2}$ ($\approx$20038 eV). If the SMMO sample is oxidized, a shift is observed in the overall spectrum toward higher binding energies. This indicates that the Mo atom has lost electrons and requires higher energies to excite subsequent electrons from the inner shells of the atom. Upon exposing the sample to the reducing environment once again, the entire spectrum shifts back towards lower edge energies at 20037 eV. This verifies that the sample is indeed reduced and gaining electrons, and thus, less energy will be required for the system to excite subsequent excess electrons. The relative $4p_{3/2}/4p_{1/2}$ ratio also gives an indication, qualitatively, about the number of allowed transitions. The oxidized sample has a ratio of about 1.17, which reveals that there are more unfilled orbital sites that allow the $1s \rightarrow 4p$ transition. The opposite is seen for the reduced SMMO sample with a ratio of around 1.08, which indicates that the system gains electrons and fills sites in the orbital that block the $1s \rightarrow 4p$ electronic transition.

Investigating the pre-edge and edge features of the XANES spectrum revealed that the Mo in SMMO has a definitive change in oxidation state if it is exposed to different reactive atmospheres. To determine the exact oxidation state of Mo in the oxidized and reduced SMMO samples, their edge energies were compared to those of molybdenum foil (Mo^0), molybdenum dioxide (Mo^{+4}), and molybdenum trioxide (Mo^{+6}) as standards (Figure 3). If the SMMO sample is completely oxidized, the $1s \rightarrow 4p_{3/2}$ transition occurs at 20038 eV, and if it is reduced the transition is shifted to 20037 eV. In comparison to the above standards, the oxidation state of molybdenum in SMMO changes from +4.67 to +4.15 upon going from the oxidized form to the reduced form (Figure 3b). Given that the SMMO material has the ability to allow multiple valent states for a single atom in its crystal structure, this can provide a pathway for electron conduction through the different molybdenum conduction bands.

Viewing the chemical formula of $Sr_2MgMoO_{6-\delta}$, it is observed that there is a "$6-\delta$" stoichiometry for oxygen. To maintain charge neutrality when the oxidation state of molybdenum changes, the concentration of oxygen in SMMO can change by "δ" through the formation of oxygen vacancies imbedded in the crystal structure. Upon oxidizing the SMMO sample ($Mo^{+4.67}$), δ will equal 0.67, and if the sample is reduced ($Mo^{+4.15}$), δ will change to 0.93. The XANES data signify that the fully oxidized SMMO sample already has built-in oxide vacancies and allows the formation of additional vacancies upon sample reduction. The presence of these oxide vacancies will induce ionic oxide conductivity to allow the oxide anions, generated at the cathode and transported through the electrolyte, to travel through these vacancies to active catalytic sites to oxidize unwanted fuel fragments.

To verify this trend in the formation of oxide vacancies, as seen in the XANES data, a Fourier transform of the EXAFS data was conducted to generate the "*R*-space" spectrum (Figure 4). Upon reducing the SMMO material, it has a Mo–O peak intensity of 1.2 $Å^{-3}$. If that same sample is exposed to compressed

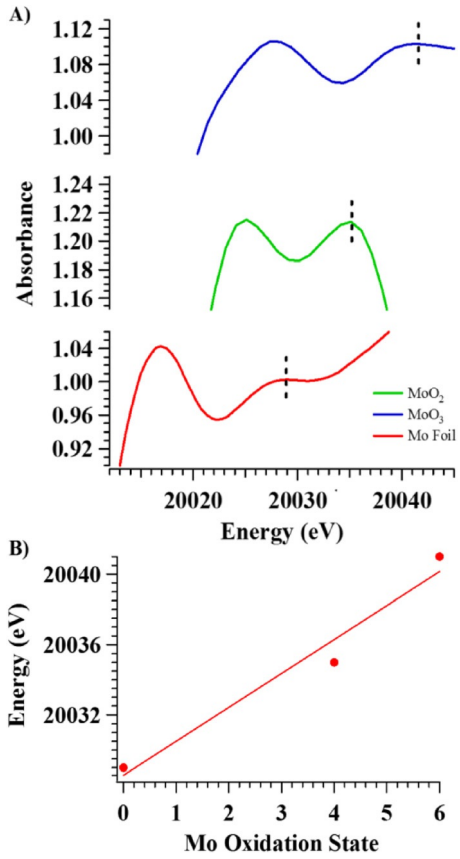

Figure 3. a) XANES spectra of molybdenum K-edge from standards of molybdenum foil (Mo^0), MoO_2 (Mo^{+4}), and MoO_3 (Mo^{+6}). The $1s \rightarrow 4p^{3/2}$ transition is highlighted in each spectrum with a dashed line. b) Calibration curve created from the linear relationship between the energy of the $1s \rightarrow 4p^{3/2}$ transition obtained from the X-ray absorption spectra in a) and molybdenum oxidation state. The above linear fit has an equation of $y = 1.9286 \pm 0.371x + 20029 \pm 1.55$.

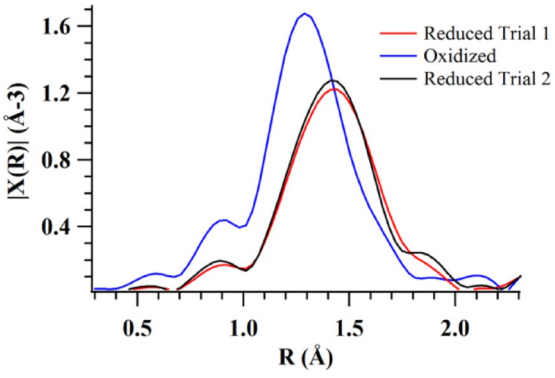

Figure 4. Fourier transform of the EXAFS spectra taken for the reduced (trial 1), oxidized, and reduced (trial 2) SMMO sample.

air, as done before, there is an increase in this peak intensity to 1.7 $Å^{-3}$. As with the XANES data, if the oxidized sample is exposed to the original reducing environment the intensity returns back to 1.2 $Å^{-3}$, and this exhibits the reversible properties of this material, as also seen in Figure 2. The equation used to model EXAFS data is listed in Equation (1). In this equation, *f*(*k*)

and $\delta(k)$ represent photoelectron scattering properties, R represents the effective distance to the neighboring atoms, and σ^2 represents the mean-square disorder of the neighbor distance. The important feature of this equation is that the intensity of this peak is directly proportional to "N", the number of neighboring atoms.[37] It is seen that for the oxidized sample there is larger intensity, 1.7 $Å^{-3}$, which signifies a larger number of oxide anions surrounding the molybdenum atom. When the oxidation state of $Mo^{+4.67}$ is reduced to $Mo^{+4.15}$, the intensity of this Mo–O peak decreases to 1.2 $Å^{-3}$, which validates that oxide vacancies localized around the molybdenum atom are being created.

$$\chi(k) = \sum_j \frac{N_j \cdot f_j \cdot (k) \cdot e^{-2k^2\sigma^2 j}}{k \cdot R_j^2} \cdot \sin\left[2kR_j + \delta_j(k)\right] \quad (1)$$

2.2. SMMO Half-Cell Membrane Electrode Assembly

Understanding how the bulk SMMO material behaves under reducing and oxidizing conditions provided a diagnostic that could be used towards the in situ measurements of SOFC assemblies that integrate SMMO as the anode material. Conducting these in situ measurements can provide vital information regarding the electronic and crystal structure of the material while under electrochemical device operation. To accomplish this task, a half-cell membrane electrode assembly (MEA) was constructed and utilized for these above purposes. In-depth details regarding the construction of the half-cell MEA is described in the Experimental Section (Figure 9). The described half cells were mounted in the custom XAS electrochemical chamber where they were exposed to a reactive atmosphere of 1:1 H_2/H_2O, each having a flow rate of 6.0 $cm^3\,min^{-1}$ at an operational temperature of 800 °C.

Figure 5 displays the electrochemical, voltammetry, and impedance measurements performed on these half cells over a range of temperatures (600–800 °C). As seen in Figure 5a, the performance of the MEA increases with increasing temperatures, as evident by the increase in current density. This attribute can have two possible scenarios: 1) electrons are conducted across the $La_{0.4}Ce_{0.6}O_{1.8}$ (LDC) electrolyte and the resistance towards these processes decreases with temperature or 2) the activation energy towards oxide anion transport across the LDC decreases with increasing temperature in a working SOFC device. To verify which scenario takes place, electrochemical impedance spectroscopy (EIS) measurements were performed on these MEAs. As seen in Figure 5b, the spectra reveal the presence of "arcs" that have both Z_{real} (resistive) and Z_{img} (capacitive) components. Specifically, the presence of Z_{img} represents capacitance in our system that is associated with a delay in charge brought upon by chemical processes taking place at the electrodes.[38–40] These EIS arcs are associated with the charge- and mass-transport processes occurring at the SMMO working electrode and platinum counter electrode.[38–40] There is also a high frequency intercept in all the spectra ranging from about 1500 Ω at 600 °C to about 160 Ω at 800 °C. These intercept values are directly proportional to the activation energy associated with the pure ohmic resistance of oxide transport through the LDC electrolyte.[38–40] From these electrochemical measurements, it is observed that these half cells are indeed working SOFC devices.

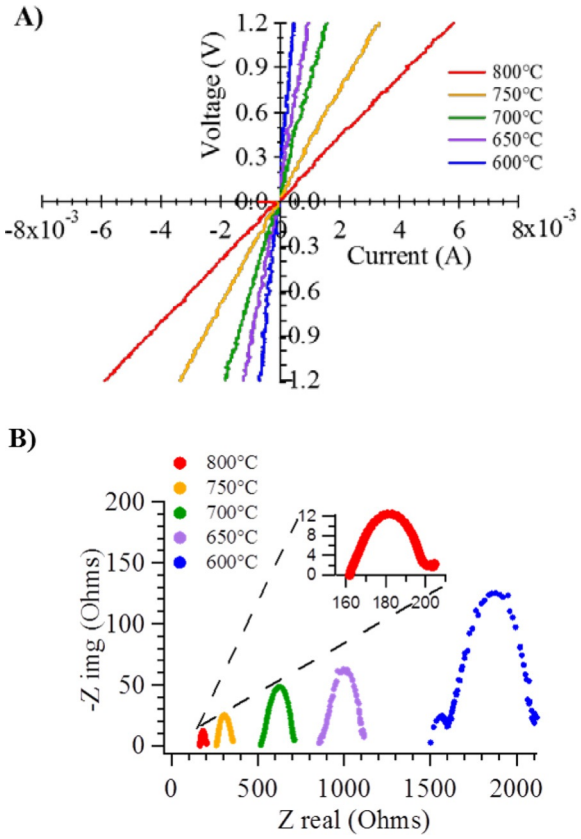

Figure 5. Electrochemical measurements of an SMMO half cell taken in the temperature range of 600 to 800 °C. a) Voltammetry with a positive bias (fuel cell H_2 oxidation) and negative bias (H_2O electrolysis) occurring at the SMMO working electrode. b) Open-circuit potential electrochemical impedance spectroscopy.

For XAS testing of the half-cell devices, the 1 mm × 1 mm X-ray beam was positioned at the SMMO/Pt current collector interface at an incidence angle of 5° to probe the TPB of this MEA. The voltage of the cell was increased from 0.0 to 1.0 V at a slow rate of 2.78×10^{-4} V s^{-1} to allow for this change to occur over 1 h (Figure 6). Simultaneously, the XAS edge spectra were taken for the reactive TPB region to observe changes in the molybdenum oxidation state with changes in cell polarization (Figure 6a). At this positive bias, the SMMO electrode performs the fuel-cell operation to oxidize H_2 with O^{2-} to create H_2O. The extent of this reaction only intensifies at higher cell potentials, at which the current of the cell increases from the counter electrode magnifying the oxide flux towards the SMMO working electrode. No variations were observed in the Mo oxidation with this voltage change, even at an extreme voltage of 1.0 V, at which the greatest oxide flux is driven towards the SMMO working electrode.

A similar experiment was conducted to generate Figure 6b, but in this case, a negative bias was applied to the SOFC so that the SMMO electrode would perform H_2O electrolysis.

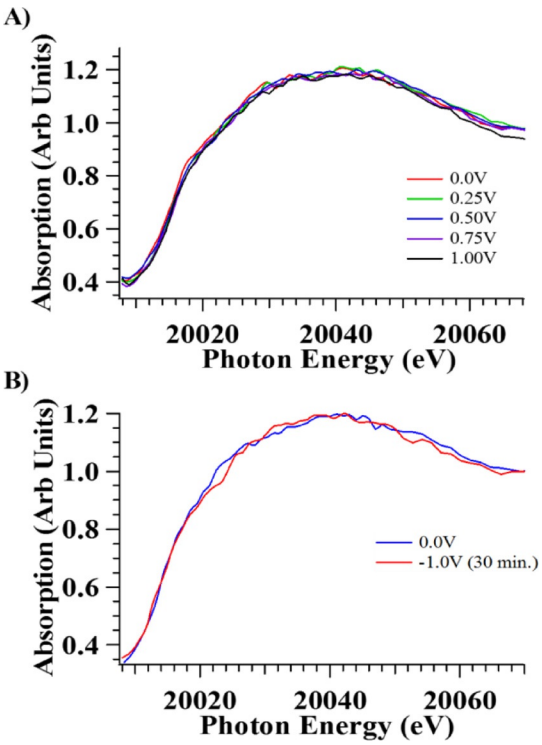

Figure 6. In situ Mo K-edge X-ray absorption spectra taken at various cell polarizations: a) positive (fuel cell) potential bias and b) negative (electrolysis) potential bias with respect to the SMMO electrode.

During this process, SMMO forms oxide anions that are directed towards the platinum counter electrode that oxidizes H_2. A voltage of −1.0 V was applied to the SOFC for 30 min. This induces the maximum amount of oxygen depletion in SMMO and drives oxygen anions towards the counter electrode to maintain the H_2 oxidation reaction taking place at the platinum electrode. As with Figure 6a, Figure 6b shows no signs of changes in the Mo oxidation state with respect to changes in the electrical potential and oxide flux concentrations. Both of these experiments exhibit that SMMO has a high stability at high cell polarizations, whether undergoing H_2 oxidation or H_2O electrolysis. In general, higher cell polarizations are beneficial to the operation of SOFCs to increase their power output and also to increase the amount of oxygen impinging on the anode to oxidize away unwanted graphite and metal sulfides that are formed.[27]

3. Conclusions

The experiments presented herein describe the use of X-ray absorption spectroscopy (XAS) in conjunction with a custom electrochemical heater assembly to allow the noninvasive exploration of Sr_2MgMoO_6 (SMMO) as an anode material at temperatures $\leq$800 °C. The roles of molybdenum were investigated for this material with regard to electron conduction and the formation of oxide vacancies. It was observed that this material had the ability to allow multiple oxidation states of Mo while still maintaining its crystal structure. The characteristic of having multivalent states in one crystal structure will help to provide the electronic conductivity needed for SMMO to be considered as an anode material. Further analysis of the extended X-ray absorption fine structure (EXAFS) data revealed that this material was also capable of creating oxide vacancies throughout its stable crystal structure, and this would allow the ionic oxide conductivity needed to block detrimental formation in the anode microstructure that can lead to eventual device failure. All of the changes that occur to the SMMO material upon oxidation were proven to be reversible processes upon reintroduction of the material into a reducing atmosphere.

Using the findings obtained from the bulk SMMO samples as a diagnostic for the in situ measurements provided insight into SMMO as an electrode in working solid-oxide fuel cell (SOFC) devices. Upon testing the SMMO half-cell, it was observed that there were no changes to the oxidation state of molybdenum in SMMO at either a positive or negative bias. All these characteristics of SMMO observed by the in situ XAS measurements revealed that SMMO can be considered an alternative SOFC anode material by providing a multivalent system to ensure electron conduction, oxide anion vacancies for fuel impurity tolerance, and stability a various cell polarizations.

The high vacuum requirements of standard X-ray instruments limit investigations to only ex situ analysis. The use of synchrotron-based XAS at the Advanced Photon Source located at Argonne National Laboratory provided similar information to that of X-ray photoelectron spectroscopy with the addition of the structural information that can be provided by the EXAFS data. Having the ability to use high-energy tunable X-rays allowed XAS measurements to be conducted in reactive environments and at elevated temperatures to mimic the operational conditions of SOFCs. The information gained from these measurements can provide direct insight into the roles that specific atoms in these materials play in oxidative fuel-cell processes during device operation. This pertinent information can also assist in the development of efficient future membrane electrode assemblies.

Experimental Section

Sr_2MgMoO_6 Perovskite Synthesis

The double perovskite Sr_2MgMoO_6 (SMMO) anode material was prepared by a solution–gel (sol–gel) synthesis technique. In this sol–gel synthesis, separate metal-ion stock solutions were created and calibrated for $Mg(NO_3)_2{\cdot}6H_2O$ and $(NH_4)_6Mo_7O_{24}{\cdot}4H_2O$ (Alfa Aesar). Stoichiometric amounts of the molybdenum and magnesium stock solutions along with anhydrous $Sr(NO_3)_2$ (Alfa Aesar) were introduced into a reaction flask with a $Sr^{2+}/Mg^{2+}/Mo^{6+}$ molar ratio of 2:1:1. This mixed metal ion solution was allowed to mix for 30 min at room temperature while the chelating agent, ethylenediaminetetraacetic acid (EDTA), was measured separately to have a metal ion to EDTA molar ratio of 1:2. The EDTA was then fully dissolved in NH_4OH (Sigma–Aldrich) before it was added slowly to the mixing metal ion solution at room temperature to create a cloudy solution. This solution was then heated to 70–80 °C and the pH of the solution was adjusted to 4.5 with HNO_3 (Sigma–Aldrich). The resulting clear solution was allowed to mix at 70–

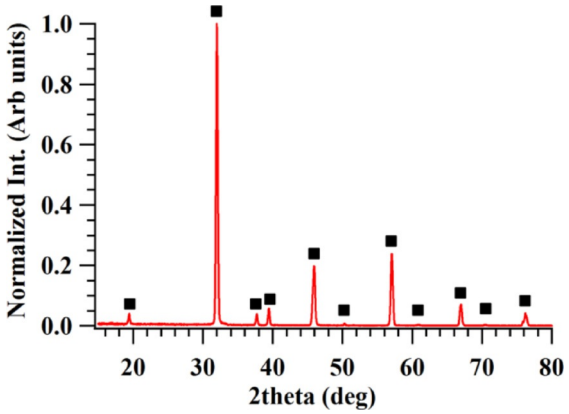

Figure 7. XRD spectrum of the single-phase SMMO material. Black squares represent placement of peaks specific to a SMMO perovskite pattern.

80 °C for 30 min to allow the chelates to undergo polyesterifcation with the metal atoms. The temperature of this solution was then increased to 90–100 °C to allow removal of the excess amount of water that resulted in an off-white viscous gel. Continued heating resulted in thermal decomposition of the gel to produce a fine gray powder. The resulting powder was collected and calcined for 6 h at 800 °C to remove excess amounts of organic residues and to leave behind metal oxide precursors as a light blue powder. This calcined product was then annealed under a reducing atmosphere of 5% H_2 diluted with Ar for 24 h at 1100 °C and for 12 h at 1200 °C, which resulted in a dark blue powder. The resulting product was characterized with X-ray powder diffraction (D8 Discover, Bruker) to verify a single phase of the (SMMO) anode material (Figure 7). The single-phase SMMO material was then pressed into 1 mm thick pellets measuring 15 mm in diameter, which were sintered at 1300 °C for 3 h. These pellets were used in the in situ fluorescence based XAS measurements studying the bulk redox chemistry of SMMO.

In Situ Fluorescence-Based XAS Chamber

A custom in situ XAS electrochemical fixture was built to allow exploration of the SMMO materials at high temperatures under reactive atmospheres by using fluorescence-based XAS measurements. This system was equipped with a ceramic substrate heater that could heat a sample up to 1100 °C under oxidizing and reducing environments. This device also incorporated multiple, hermetic

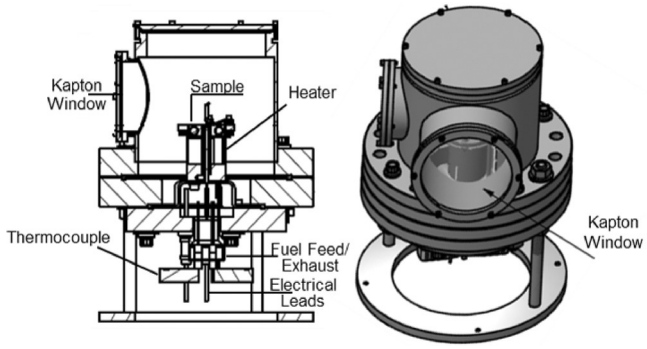

Figure 8. Schematic design of the SOFC architecture used in the majority of in situ XAS experiments. Left) Cross section of chamber showing components. Right) 3D representation of in situ XAS chamber.

electrical feedthroughs that permitted both temperature and electrochemical measurements and control of the cell throughout the study. Inlet and outlet gas ports were also integrated into the chamber to control flow of either a reducing (3% H_2 in 97% He) or oxidizing (air) environment. There was a top removable flange that allowed new samples to be introduced and old samples to be removed. This chamber was also equipped with two X-ray transmissive Kapton windows positioned 90° from each other to allow for X-ray radiation to enter the chamber, interact with the sample, and allow scattered photons to leave the chamber to be recorded by a Lytle detector. This system allowed exploration of the redox chemistry of the SMMO electrode material at elevated temperatures (≥800 °C) while also under electrochemical control from various cell polarizations. A schematic of the described system can be seen in Figure 8.

Bulk SMMO Redox Chemistry

To first understand the limits of reduction and oxidation for SMMO at 800 °C, preliminary XAS measurements were taken of bulk SMMO pellets utilizing the in situ XAS chamber. SMMO pellets were created by loading a 15 mm pressing die with 1 g of SMMO powder and pressing at 69 MPa for 5 min. The resulting pellet was sintered at 1300 °C under a 5% H_2 atmosphere for 5 h. The pellet was mounted to the substrate heater in the in situ XAS chamber and was heated to 800 °C under a 3% H_2 (diluted in helium) environment at 200 $cm^3 min^{-1}$. Continuous spectra were taken for 1 h to ensure a steady state was reached for the reduced SMMO sample. This chamber was then purge with helium to evacuate any H_2 before air was applied to the chamber at 200 $cm^3 min^{-1}$ to oxidize the SMMO sample. Continuous spectra were once again taken for 1 h to ensure a steady state was reached for the oxidized SMMO sample. This process was repeated to ensure redox reversibility from switching back and forth from the hydrogen (reducing) and air (oxidizing) atmospheres.

SOFC Half-Cell Construction and Experiment

To explore the effects that cell potentials and different oxide anion fluxes had on the SMMO anode materials, these materials were integrated into working SOFC devices by utilizing a "half-cell" geometry. An $La_{0.4}Ce_{0.6}O_{1.8}$ (LDC) electrolyte substrate first needed to be created. This powder was created by using solid-state synthesis in which stoichiometric ratios of La_2O_3 and CeO_2 were mixed homogenously and treated at 1250 °C for 10 h. To create the LDC electrolyte, 3.0 g were loaded into a 30 mm pressing die and pressed at 69 MPa for 5 min. The resulting LDC pellet was sintered at 1450 °C for 10 h to produce a 1 mm thick, 25 mm diameter electrolyte. To this LDC electrolyte, a 1 μm thick SMMO working electrode was aerosol printed with a length and width of 8 mm and 4 mm. The electrode ink formula consisted of the following chemicals and mass percentages: 34.5% SMMO, 9.5% α-terpineol, 54.0% 2-butanol, 0.2% ethyl cellulose 300, 0.6% disperbyk 111, 0.4% polyalkyl glycol, 0.4% polyvinyl butyral, and 0.4% butyl benzyl phthalate. For information about aerosol printing parameters, refer to Sukeshini et al.[41] This SMMO working electrode was then sintered at 1300 °C for 5 h. A platinum counter electrode with dimensions of 4 mm × 8 mm × 200 nm was sputtered 2 mm away from the SMMO working electrode. Platinum current collectors with gold wire were then attached to each electrode and dried at 150 °C for 5 h. A depiction of this half cell is shown in Figure 9. Figure 9 also exhibits the reactions taking place at each electrode if a positive bias is applied to the SOFC upon exposure to a reactive environment of 1:1

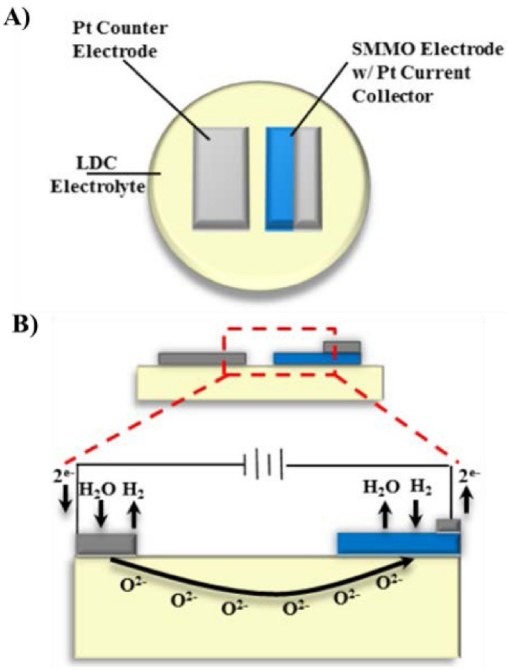

Figure 9. Schematic of a working SMMO half-cell MEA. a) Graphic represents an aerial view of the MEA. b) Graphic corresponds to a cross section of the MEA. Reaction presented in the figure correlates to application of a positive bias to the SMMO working electrode.

H_2/H_2O (6.0/6.0 $cm^3 min^{-1}$). This reactive environment was supplied by a 200 $cm^3 min^{-1}$ 3% H_2 in 97% He fuel feed that passed through an H_2O bubbler at room temperature to produce an approximately 3.0% humidified fuel feed (6.0 $cm^3 min^{-1}$ of H_2O).

As seen in Figure 9, if a positive bias is applied to the half cell, the SMMO working electrode undergoes H_2 oxidation and also supplies a steady flow of electrons to the counter platinum electrode to assist in H_2O electrolysis, which will then create oxide anions that will be electrochemically driven back to the working electrode to complete the circuit. The roles of the working and counter electrodes are reverse if a negative bias is applied to the cell. Successful experiments similar to these have been conducted by researchers at the University of Maryland and The Lawrence Berkeley National Laboratory, for which a half cell MEA was created to look at cerium oxidation states with ambient-pressure X-ray photoelectron spectroscopy.[42]

Acknowledgements

This research was supported by the National Academies of Sciences through the Research Associateship Program. Funding for this research was provided through the Air Force Research Laboratory, Wright-Patterson Air Force Base. Access to the 10-ID beamline at the Advanced Photon Source located at Argonne National Laboratory was granted through proposal GUP-28614. MRCAT operations are supported by the Department of Energy and the Materials Research Collaborative Access Team (MRCAT) member institutions.

Keywords: electrochemical impedance spectroscopy · fuel cells · linear-sweep voltammetry · perovskites · X-ray absorption spectroscopy

[1] R. Ormerod, *Chem. Soc. Rev.* **2003**, *32*, 17 – 28.
[2] C. Song, *Catal. Today* **2002**, *77*, 17 – 49.
[3] M. Pomfret, O. Demircan, A. Sukeshini, R. Walker, *Environ. Sci. Technol.* **2006**, *40*, 5574 – 5579.
[4] A. Appleby, *J. Power Sources* **1996**, *58*, 153 – 176.
[5] B. Eigenbrodt, R. Walker, *Anal. Methods* **2011**, *3*, 1478 – 1484.
[6] J. Kirtley, B. Eigenbrodt, R. Walker, *ECS Trans.* **2011**, *33*, 25 – 37.
[7] H. Zhu, R. Kee, V. Janardhanan, O. Deutschmann, D. Goodwin, *J. Electrochem. Soc.* **2005**, *152*, A2427 – A2440.
[8] M. Pomfret, J. Owrutsky, R. Walker, *Anal. Chem.* **2007**, *79*, 2367 – 2372.
[9] M. Pomfret, C. Stoltz, B. Varughese, R. Walker, *Anal. Chem.* **2005**, *77*, 1791 – 1795.
[10] K. Swider, W. Worrell, *J. Electrochem. Soc.* **1996**, *143*, 3706 – 3711.
[11] N. Sammes, Z. Cai, *Solid State Ionics* **1997**, *100*, 39 – 48.
[12] J. Lee, S. Yoon, B. Kim, J. Kim, H. Lee, H. Song, *Solid State Ionics* **2001**, *144*, 175 – 184.
[13] A. Svensson, S. Sunde, K. Nisancioglu, *J. Electrochem. Soc.* **1998**, *145*, 1390 – 1400.
[14] J. Nielsen, T. Jocobsen, *Solid State Ionics* **2008**, *178*, 1769 – 1776.
[15] H. Fukunaga, M. Ihara, K. Sakaki, K. Yamada, *Solid State Ionics* **1996**, *86 – 88*, 1179 – 1185.
[16] A. Martinez, J. Brouwer, *J. Power Sources* **2010**, *195*, 7268 – 7277.
[17] B. Kenney, M. Valdmanis, C. Baker, J. Pharoah, K. Karan, *J. Power Sources* **2009**, *189*, 1051 – 1059.
[18] V. Janardhanan, V. Heuveline, O. Deutschmann, *J. Power Sources* **2008**, *178*, 368 – 372.
[19] W. Zhu, D. Ding, C. Xia, *Electrochem. Solid-State Lett.* **2008**, *11*, B83 – B86.
[20] M. Schmidt, K. Hansen, K. Norrman, M. Mogensen, *Solid State Ionics* **2009**, *180*, 431 – 438.
[21] J. Erning, T. Hauber, U. Stimming, K. Wippermann, *J. Power Sources* **1996**, *61*, 205 – 211.
[22] J. Goodenough, *Annu. Rev. Mater. Res.* **2003**, *33*, 91 – 128.
[23] K. Dietzel, J. Campbell, M. Bartlett, *J. Chromatogr. A* **2005**, *1093*, 11 – 20.
[24] M. Gong, X. Liu, J. Trembly, C. Johnson, *J. Power Sources* **2007**, *168*, 289 – 298.
[25] Y. Huang, R. Dass, Z. Xing, J. Goodenough, *Science* **2006**, *312*, 254 – 257.
[26] C. Sun, U. Stimming, *J. Power Sources* **2007**, *171*, 247 – 260.
[27] B. Eigenbrodt, M. Pomfret, D. Steinhurst, J. Owrutsky, R. Walker, *J. Phys. Chem. C* **2011**, *115*, 2895 – 2903.
[28] M. Pomfret, J. Owrutsky, R. Walker, *J. Phys. Chem. B* **2006**, *110*, 17305 – 17308.
[29] A. Bieberle, L. Meier, L. Gauckler, *J. Electrochem. Soc.* **2001**, *148*, A646 – A656.
[30] S. Bebelis, S. Neophytides, *Solid State Ionics* **2002**, *152 – 153*, 447 – 453.
[31] A. Bieberle, L. Meier, L. Gauckler, *Solid State Ionics* **2002**, *146*, 23 – 41.
[32] S. Sundes, *Electrochim. Acta* **1997**, *42*, 2637 – 2648.
[33] A. Kuzmin, J. Puran, *Radiat. Meas.* **2001**, *33*, 583 – 586.
[34] S. Vasala, M. Lehtimaki, S. Haw, J. Chen, R. Liu, H. Yamauchi, M. Karppinen, *Solid State Ionics* **2010**, *181*, 754 – 759.
[35] F. Vila, J. Rehr, H. Rossner, H. Krappe, *Phys. Rev. B* **2007**, *76*, 014301.
[36] F. Lima, R. Bjornsson, T. Weyhermuller, C. Perumalreddy, P. Glatzel, F. Neese, S. Debeer, *Phys. Chem. Chem. Phys.* **2013**, *15*, 20911 – 20920.
[37] T. Chan, R. Liu, L. Jang, *J. Chin. Chem. Soc.* **2005**, *52*, 721 – 724.
[38] W. Bessler, *Solid State Ionics* **2005**, *176*, 997 – 1011.
[39] P. Hofmann, K. Panopoulos, *J. Power Sources* **2010**, *195*, 5320 – 5339.
[40] A. Bieberle, L. Gauckler, *Solid State Ionics* **2000**, *135*, 337 – 345.
[41] A. Sukeshini, F. Meisenkothen, P. Gardner, T. Reitz, *J. Power Sources* **2013**, *224*, 295 – 202.
[42] C. Zhang, M. Grass, A. McDaniel, S. DeCaluwe, F. Gabaly, Z. Liu, K. McCarty, R. Farrow, M. Linne, Z. Hussain, G. Jackson, H. Bluhm, B. Eichhorn, *Nature* **2010**, *9*, 944 – 94.

Manuscript received: June 30, 2015
Final Article published: August 5, 2015